Fingerprints of the Crossing of the Frenkel and Melting Line on the Properties of High-Pressure Supercritical Water.

Ioannis Skarmoutsos [a,*], Jannis Samios [b] and Elvira Guardia [c]

[a] *Laboratory of Physical Chemistry, Department of Chemistry, University of Ioannina, 45110 Ioannina, Greece*
[b] *Department of Chemistry, Laboratory of Physical Chemistry, National and Kapodistrian University of Athens, Panepistimiopolis 157-71, Athens, Greece*

[c] *Departament de Física, Universitat Politècnica de Catalunya, Campus Nord-Edifici B4-B5, Jordi Girona 1-3, Barcelona E-08034, Spain.*

Abstract

Using molecular dynamics simulations in combination with the two-phase thermodynamic model, we reveal novel characteristic fingerprints of the crossing of the Frenkel and melting line on the properties of high-pressure water at a near critical temperature (1.03 T_c). The crossing of the Frenkel line at about 1.17 GPa is characterized by a crossover in the rotational and translational entropy ratio S^{rot}/S^{trans}, indicating a change in the coupling between translational and rotational motions which is also reflected on the shape of the rotational density of states. The observed isosbestic points in the translational and rotational density of states are also blue-shifted at density and pressure conditions higher than the ones corresponding to the Frenkel line. The first-order phase transition from a rigid liquid to a face-centered cubic plastic crystal phase at about 8.5 GPa is reflected on the discontinuous changes in the translational and rotational entropy, particularly on the significant increase of the ratio S^{rot}/S^{trans}. A noticeable discontinuous increase of the dielectric constant has also been revealed when crossing this melting line, atrributed to the different arrangement of the water molecules in the plastic crystal phase. The reorientational dynamics in the plastic crystal phase is faster in comparison with the 'rigid' liquid-like phase, but remains unchanged upon a further pressure increase in the range 8.5-11 GPa.

[*] Corresponding author: iskarmoutsos@uoi.gr

Supercritical fluids have attracted significant interest in diverse areas of science and engineering, due to their unique physicochemical properties and corresponding applications[1]. Particularly during the last decade, the study of the fundamental properties and the nature of supercritical fluids has received a new, noticeable attention from the scientific community. The main reason for this is that recent experimental and theoretical evidences started questioning the generally accepted idea that the supercritical region is a single fluid phase region[2-19]. Based on these evidences, several characteristic lines have been defined in order to divide the supercritical thermodynamic phase space into different regimes[2-16]. However, when crossing these lines, first- or second-order phase transitions, characterized by discontinuous changes in the thermodynamic properties of the fluids, are not observed. The crossing of these lines is characterized either by local extrema or crossovers in several thermodynamic quantities, where significant but not abrupt changes of these properties can be observed. The first line introduced in the literature in order to distinguish different regimes in the supercritical thermodynamic phase space was the Widom line[2-10]. The Widom line, originating from the critical point, identifies the boundary between two different regimes where supercritical fluids are characterized as gas-like and liquid-like fluids, respectively. Note that the definition of the Widom line is not unique and it depends upon the identification of the local maxima of thermodynamic response functions, such as the constant pressure specific heat C_p, the thermal expansion coefficient α_p and the isothermal compressibility K_T, along different isobars or isotherms[10]. The crossing of the Widom line is often characterized in the literature as supercritical pseudo-boiling[7,20] and our previous studies[21] have pointed out that it is also related to the existence of significant local density inhomogeneities[17,22] in supercritical fluids. At higher pressures, supercritical fluids exhibit crossovers in several properties, often characterized by the introduction of a new line called the Frenkel line[12-16]. The Frenkel line has been characterized as the boundary between a “non-rigid” liquid-like fluid and a “rigid” liquid and it is essentially different than the Widom line. However, it should be noted that the criteria used to identify the Frenkel line up to know have been a subject of debate[23-25] and an active area of research[21, 26-31] in order to provide deeper insights of the molecular-scale phenomena taking place at high pressures.

In a very recent work[21], we focused on supercritical water (SCW) and revealed with the aim of molecular dynamics and Monte Carlo simulation techniques that a near-critical isotherm can be divided into different domains where SCW exhibits distinct behavior, ranging from a gaslike to a plastic crystal one. By investigating a wide range of structural, thermodynamic, and dynamic properties of SCW, we provided solid evidence about the existence of a structural transition from a liquidlike fluid to a compressed, tightly packed liquid, in the density and pressure region around 3.4 ρ_c and 1.17 GPa, introducing an alternative approach to locate the crossing of the Frenkel line. Moreover, at much higher pressures, around 8.5 GPa, we observed another first-order phase transition to a face-centered cubic (fcc) plastic crystal polymorph. Such an observation clearly reveals the existence of a melting line of water at supercritical conditions, which is located at very elevated pressures.

Motivated by all the previous findings, we focused on the role of entropy and related dynamics of SCW in the range of thermodynamic conditions where the crossing of the Frenkel and melting lines is observed. SCW has been selected to be studied due to is great importance in a wide range of phenomena in chemistry, physics, materials and earth-planetary science. In our previous study[21] we observed a crossover in a rotational-translational coupling parameter when crossing the Frenkel line along a near-critical isotherm of SCW. Such an observation indicates that the balance between translational and rotational motions changes when the structural transition from a “non-rigid” to a “rigid” liquid takes places.

At higher pressures, when the first-order transition from a “rigid” liquid to a plastic crystal phase takes place, the individual water molecules are still able to rotate. On the other hand, the translational motions are limited to low-frequency oscillations around the lattice sites, reflected on the very short-time scale behavior of their velocity time correlation functions. From a thermodynamic point of view, it is well known from the literature that the fingerprints of the different types of molecular motions on the entropy of a molecular system can be revealed by applying the two-phase thermodynamic model[32,33]. With the aim of this particular statistical mechanical model the translational and rotational components of the total entropy of the system can be directly extracted. In this way, the changes in the

relative contributions of each component when crossing the Frenkel and the melting line can provide important information about the effect of these different type of entropic driving forces on these phenomena.

The two-phase thermodynamic (2PT) model has been presented in details in previous works in the literature[32,33]. Briefly speaking, the 2PT model relies upon the calculation of total density of states (DOS) function $s(\nu)$:

$$s(\nu) = \frac{2}{k_B T} \sum_{j=1}^{N} \sum_{k=1}^{3} m_j \cdot s_j^k(\nu) \tag{1}$$

In this equation m_j is the mass of atom j, N is the total number of atoms of the system and $s_j^k(\nu)$ the spectral density of atom j in the k axis direction (k = x, y, and z in a Cartesian coordinate system), which is defined as:

$$s_j^k(\nu) = \lim_{\tau \to \infty} \frac{1}{2\tau} \left| \int_{-\tau}^{\tau} v_j^k(t) \cdot e^{-i2\pi\nu t} dt \right|^2 \tag{2}$$

where $v_j^k(t)$ is the k-component of the velocity vector of atom j at time t. In the case of rigid polyatomic molecular systems, where the vibrational degrees of freedom are frozen, the total DOS can be decomposed into a translational and a rotational component:

$$s(\nu) = s_{trans}(\nu) + s_{rot}(\nu) \tag{3}$$

The translational component is determined from the molecular center of mass velocities, using an analogous expression with Eq. 1, 2, whereas the rotational component from the angular velocity:

$$s_{rot}(\nu) = \frac{1}{k_B T} \sum_{l=1}^{M} \sum_{k=1}^{3} \lim_{\tau \to \infty} \frac{I_l^k}{\tau} \left| \int_{-\tau}^{\tau} \omega_l^k(t) \cdot e^{-i2\pi\nu t} dt \right|^2 \tag{4}$$

In Eq. 4 I_l^k and ω_l^k are the moment of inertia and the angular velocity of molecule l about the k principal axis of inertia, respectively. M in Eq. 4 is the total number of molecules in the system. The translational and rotational DOS can also be decomposed into a gas-like and a solid-like component, respectively:

$$s_{trans}(\nu) = {s_{trans}}^{g}(\nu) + {s_{trans}}^{s}(\nu) \quad , \quad s_{rot}(\nu) = {s_{rot}}^{g}(\nu) + {s_{rot}}^{s}(\nu) \tag{5}$$

The gas-like components are expressed as:

$${s_{trans}}^{g}(\nu) = \frac{s_{trans}(0)}{1+\left(\frac{\pi \cdot s_{trans}(0) \cdot \nu}{6 \cdot f_{trans} \cdot N}\right)^2} \quad , \quad {s_{rot}}^{g}(\nu) = \frac{s_{rot}(0)}{1+\left(\frac{\pi \cdot s_{rot}(0) \cdot \nu}{6 \cdot f_{rot} \cdot N}\right)^2} \tag{6}$$

where f_{Trans} and f_{Rot} are the translational and rotational fluidicities, defined in details in previous works in the literature[32,33]. Briefly speaking, the translational and rotational fluidicity correspond to the fractions of the total translational and rotational degrees of freedom of the system, respectively, which can be described as 'gas-like' degrees of freedom. As it has been systematically presented in the literature[32,33], they can be obtained by the following equation:

$$2 \cdot {\Delta_i}^{-9/2} \cdot {f_i}^{15/2} - 6 \cdot {\Delta_i}^{-3} \cdot {f_i}^{5} - {\Delta_i}^{-3/2} \cdot {f_i}^{7/2} + 6 \cdot {\Delta_i}^{-3/2} \cdot {f_i}^{5/2} + 2 \cdot f_i - 2 = 0 \tag{7}$$

The dimensionless diffusivity constant is expressed as:

$$\Delta_i\left(T, V, N, m, s_i(0)\right) = \frac{2 \cdot s_i(0)}{9N} \cdot \left(\frac{\pi \cdot k_B \cdot T}{m}\right)^{1/2} \cdot \left(\frac{N}{V}\right)^{1/3} \cdot \left(\frac{6}{\pi}\right)^{2/3}, \quad i = trans, rot \tag{8}$$

In the framework of the 2PT model, a thermodynamic property Φ (e.g., the entropy S) can be expressed as a functional of the gas-like and the solid-like components of the total DOS $s(\nu)$:

$$\Phi = \int_0^\infty s^g(\nu) \cdot W_\Phi^g(\nu) \cdot d\nu + \int_0^\infty s^s(\nu) \cdot W_\Phi^s(\nu) \cdot d\nu \tag{9}$$

The weighting functions $W_\Phi^g(\nu)$ and $W_\Phi^s(\nu)$ corresponding to different thermodynamic properties Φ are presented in details in previous works in the literature[32,33]. In Eq. 9, in the case of rigid polyatomic molecules, the gas-like and solid-like components of the total DOS are expressed as:

$$s^g(\nu) = {s_{trans}}^{g}(\nu) + {s_{rot}}^{g}(\nu) \quad , \quad s^s(\nu) = {s_{trans}}^{s}(\nu) + {s_{rot}}^{s}(\nu) \tag{10}$$

By decomposing the gas- and solid-like components of the total DOS into their translational and rotational components, Eq. 9 can be re-written as:

$$\Phi = \int_0^\infty \left({s_{trans}}^g(\nu) \cdot W_\Phi^g(\nu) + {s_{trans}}^s(\nu) \cdot W_\Phi^s(\nu) \right) \cdot d\nu + \int_0^\infty \left({s_{rot}}^g(\nu) \cdot W_\Phi^g(\nu) + {s_{rot}}^s(\nu) \cdot W_\Phi^s(\nu) \right) \cdot d\nu = \Phi^{trans} + \Phi^{rot} \quad (11)$$

In this way, a thermodynamic property Φ can be decomposed into its translational and rotational components Φ^{trans} and Φ^{rot}, respectively.

In the present study we focused on the behavior of the entropy S of fluid SCW and its translational and rotational components, S^{trans} and S^{rot}, along a near-critical isotherm (T=1.03 T_c, T_c = 647.1 K,) and in the density range 2.2-4.8 ρ_c (ρ_c = 0.322 g/cm^3), which corresponds to the high-pressure range of 0.12-7.06 GPa. Subsequently, we focused on the entropic changes when crossing the melting line of SCW at 8.5 GPa, where a first-order transition from a metastable liquid-like phase with density 4.976 ρ_c to a fcc plastic crystal phase with density 5.178 ρ_c takes place[21]. The properties of the fcc plastic crystal phase of water were also investigated at the densities of 5.235 ρ_c, 5.339 ρ_c and 5.434 ρ_c, corresponding to the pressures of 9, 10 and 11 GPa, respectively. Molecular dynamics (MD) simulations in the NVT ensemble were performed for all the range of the investigated densities, using the SPC/E potential model of water[34]. The densities of the fcc plastic crystal phase corresponding to 9, 10 and 11 GPa were calculated by first performing MD simulations in the NPT ensemble. Previous systematic studies have verified the accuracy of the SPC/E model in estimating the critical point of water as well as various thermodynamic, structural, transport and dynamic properties of the system[21,35-38]. The investigated temperature is also higher than the predicted critical temperature of SPC/E water, ensuring that the simulated system is at supercritical conditions. Well equilibrated initial configurations of 500 water molecules in cubic boxes corresponding to the investigated densities, from previous 15 ns MD runs, have been used in subsequent 5 ns MD runs using the DL_POLY code[39]. A 9 Å cutoff was used in the simulations to treat the van der Waals interactions, while the long-range electrostatic interactions were treated using the standard Ewald summation method[40]. The equations of motion in the MD simulations were integrated using a leapfrog-type Verlet algorithm[40] and the integration

time step was set to 1 fs. The intramolecular geometry of the water molecules was constrained using the shake algorithm and the temperature (in the case of NVT-MD simulations) and pressure (in the case of NPT-MD simulations) were constrained using Nose-Hoover thermostats and barostats[41,42], respectively. The simulation trajectories, containing the atomic positions and velocities, were further analyzed using the DoSPT code[43], where the 2PT model is implemented.

The density dependence of the translational, rotational and total entropy of fluid SCW, in the density range 2.2-4.8 ρ_c, as well as the density and pressure dependence of the fraction S^{rot} / S^{trans} is presented in Figure 1. From this figure it can be seen that both the translational and rotational entropy of SCW, as well as their sum, decrease with the increase of the density. However, the ratio S^{rot} / S^{trans} remains almost constant, exhibiting values slightly fluctuating around 0.46, up to about 3.4 ρ_c and 1.17 GPa. At higher densities and pressures, the ratio S^{rot} / S^{trans} starts to increase, as it be clearly seen in Figure 1. Interestingly, in previous studies[44] of confined water in a series of carbon nanotubes of different diameter, it was observed that when the nanotube diameter decreases, the fraction of S^{rot} / S^{trans} increases. In the cases of (8,8) and (7,7) nanotubes this fraction is close to the value obtained for bulk liquid water (≈ 0.21)[33]. However, the situation changes for the narrower (6,6) nanotubes where the fraction of S^{rot} / S^{trans} obtains the value of about 0.43, a value very similar to the one obtained in our study for the density range 2.2-3.4 ρ_c . Moreover, in the (6,6) nanotube case, due to the single-file diffusion of the water molecules in the tube, the Fourier transform of the component of the velocity time correlation function (tcf) which is transverse to the tube axis exhibits a peak. Such a peak has also been observed for the spectral density of the transverse current tcf when crossing the Frenkel line[45], since at densities higher at the one corresponding to the Frenkel line supercritical systems sustain propagating solid-like transverse modes. Interestingly, the ratio of S^{rot} / S^{trans} when these two different types of structural transitions, which however exhibit some very characteristic analogies, take place is very similar. However, in order to provide deeper and more quantitative insight on the interrelation between each component of the system's entropy and the system's density, pressure and local structural order/phase behavior, the development of new theoretical models is required.

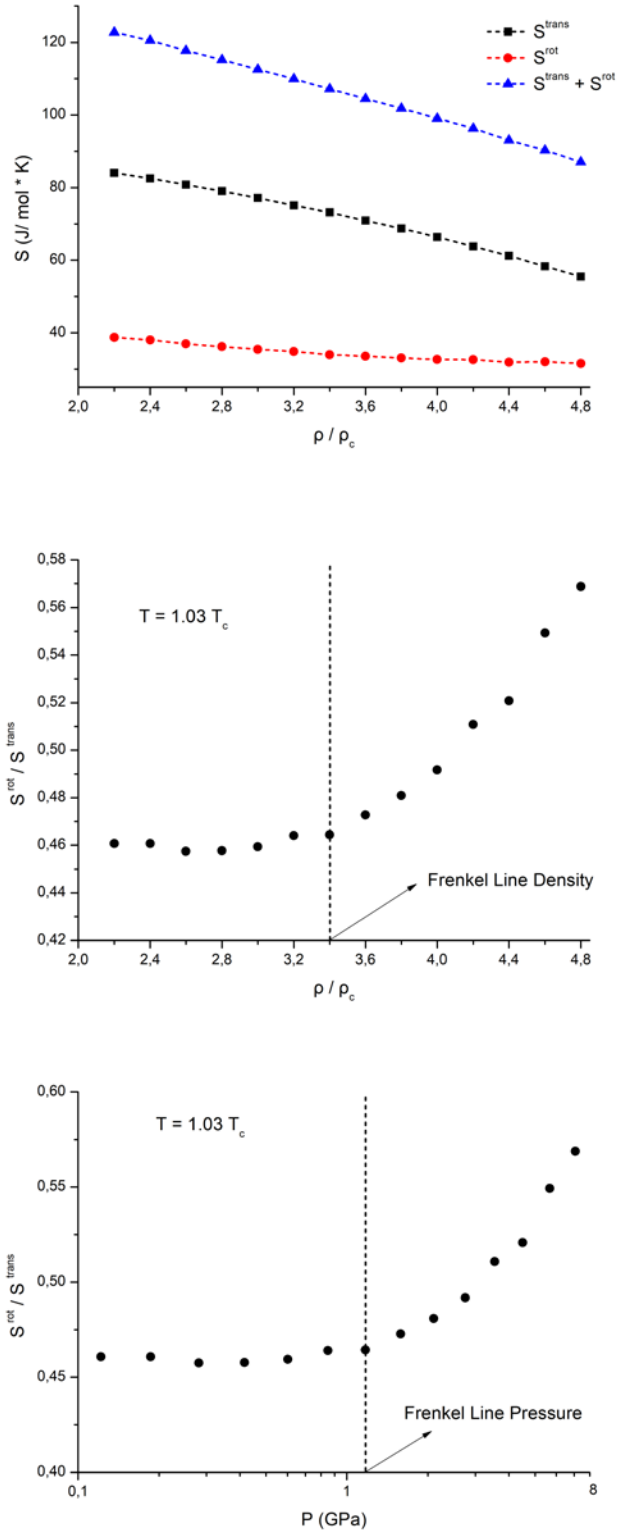

Figure 1: Density and pressure dependence of S^{rot}, S^{trans}, their sum and ratio when going from the non-rigid liquid-like phase to the rigid liquid-like phase.

The crossover of the ratio of the rotational and translational entropy of water, S^{rot} / S^{trans}, observed at 3.4 ρ_c and 1.17 GPa provides a thermodynamically-based evidence that the crossing of the Frenkel line of SCW at this particular isotherm is located at these specific conditions, a finding which is in agreement with our recent studies[21]. In those studies, we had observed another crossover of a rotation-translation coupling parameter[21] $\alpha^{rot/trans}$, indicating that when crossing the Frenkel line of SCW the rotational motions of the water molecules start to become more pronounced than the translational ones. This is clearly reflected on the density dependence of the ratio S^{rot} / S^{trans}, providing a thermodynamically-based evidence of the changes in these molecular-scale phenomena associated to the crossing of the Frenkel line. Note also that a previous simulation study by Yoon et al.[31], using the TIP4P/2005 water potential model and also employing the 2PT model, had also predicted the existence of the Frenkel line in SCW at very high temperatures (in the range 2.0-5.0 T_c). The location of the Frenkel line in the previous studies was based on the inflection point of the curve $f_{trans}(\rho)$, describing the density dependence of the translational fluidicity. Our present work, focusing on the entropic phenomena taking place in SCW at a near critical isotherm points out for the first time the role of the partition of the total entropy of the system into translational and rotational components, as reflected on the ratio S^{rot} / S^{trans}, on the structural transitions associated to the crossing of the Frenkel line. Interestingly, the locations of the crossing of the Frenkel line at the 1.03 T_c isotherm using as descriptors either the S^{rot} / S^{trans} ratio or the rotation-translation coupling parameter $\alpha^{rot/trans}$ coincide. These predictions are also in very good agreement with the results of Trachenko and co-workers[16], at least at the near-critical isotherm investigated in the present study, using the changes in the molecular velocity tcf as a descriptor. On the other hand, as pointed out by Yoon et al, the location of the Frenkel line using the translational fluidicity as a descriptor exhibits some small differences with the predictions of Trachenko and co-workers[15,16]. All these findings are strong indications of the role of the rotational motions of the water molecules on the structural transitions associated to the Frenkel line.

The changes in the rotational motions of the water molecules when crossing the Frenkel line are also reflected on the rotational DOS $s_{rot}(\nu)$, presented in Figure 2. In this figure it can be seen that at densities higher than 3.4 ρ_c a shoulder located at about 800 cm^{-1} appears

in the rotational DOS, which is blue-shifted at 900 cm^{-1} at higher densities. Another interesting feature is observed, regarding the observed isosbestic points in the rotational and translational DOS, presented in Figure 2, when crossing the Frenkel line. According to the literature[46], when plotting nonmonotonic curves $s(\nu,\rho)$ as a function of frequency ν and density ρ (ρ is each simulated density of SCW), their crossing points are located along a curve $\nu^*(\rho)$, defined as:

$$\left.\frac{\partial s(\nu,\rho)}{\partial \rho}\right|_{\nu^*(\rho)} = 0 \tag{12}$$

If these intersection points are confined in a narrow region, then the value $\nu^*(\rho)$ depends only weak on ρ. In such a case we refer to them as isosbestic points. Particularly in the case where the curves intersect at a single point ν_0, $\nu^*(\rho)$ does not depend on ρ at all and the isosbestic point ν_0 is defined as:

$$\left.\frac{\partial s(\nu,\rho)}{\partial \rho}\right|_{\nu_0} = 0 \tag{13}$$

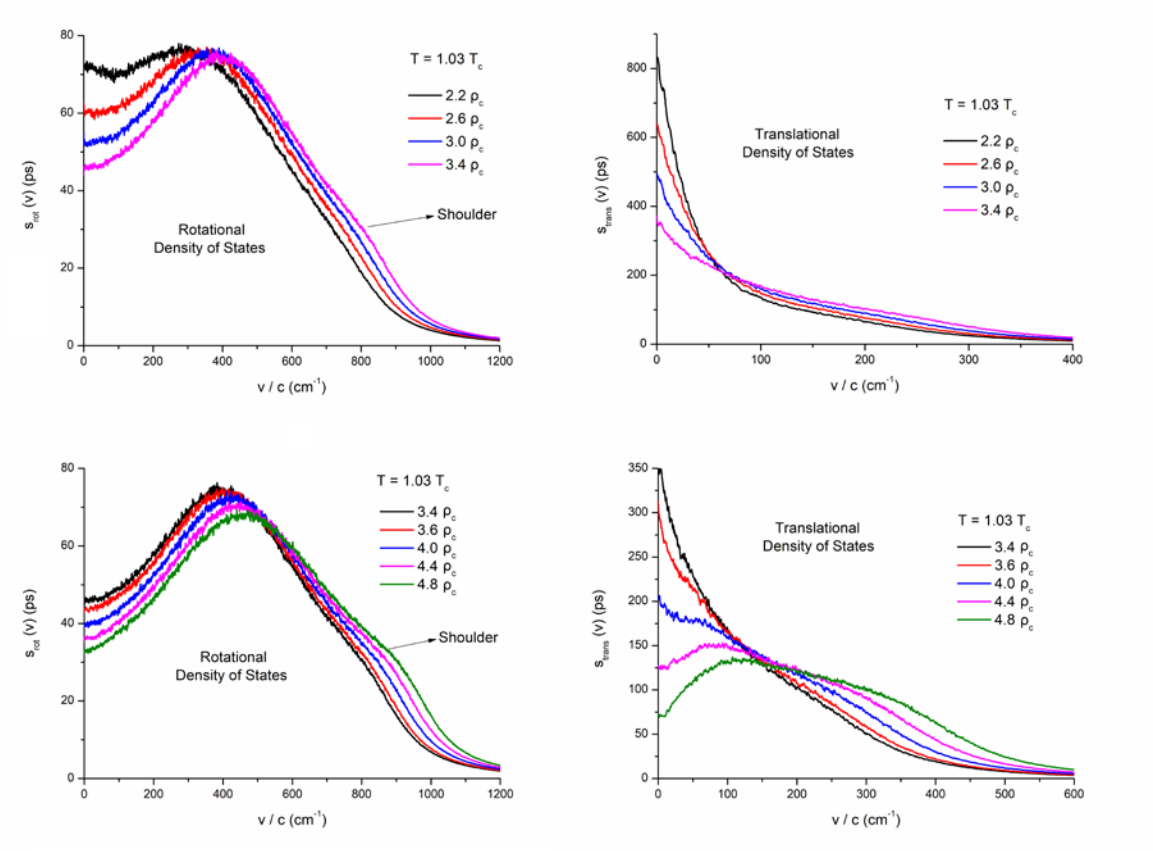

Figure 2: Calculated rotational and translational density of states of supercritical water.

In the density range 2.2-3.4 ρ_c an isosbestic point is observed for all the calculated rotational DOS $s_{rot}(v,\rho)$ at about $v_0 / c = 360 \ \ cm^{-1}$ (c is the speed of light). Interestingly at densities higher than 3.4 ρ_c, this isosbestic point is blue-shifted to $v_0 / c = 510 \ \ cm^{-1}$. Such a behavior is also clearly observed in the case of the calculated translational DOS $s_{trans}(v,\rho)$ presented in Figure 2. In the density range 2.2-3.4 ρ_c an isosbestic point is located at about $v_0 / c = 65 \ \ cm^{-1}$, whereas at higher densities the isosbestic point is shifted to $v_0 / c = 165 \ \ cm^{-1}$. Previous works in the literature have focused on isosbestic points of spectral functions in systems consisted of different components, with distinct fractions being in equilibrium among them. These components can be e.g., different types of local structures in non-reactive fluids or precursors and products of chemical reactions in

reactive systems. The overall contribution of all these components gives the total spectral observable. The shift in the frequencies of well-observed isosbestic points at different regions of the thermodynamic phase-space could be attributed to changes of the actual components and the appearance of new ones, according to the literature[47].

Note that in our previous studies[21] we revealed that around the Frenkel line, several structural order parameters exhibit significant changes. The tetrahedral[48] and trigonal[49] order parameters are maximized at the Frenkel line boundary and at higher densities they decrease. The loss of this particular orientational order, which is one of the most characteristic features of ambient and supercooled liquid water and ice, is caused by the very dense packing of the molecules at short intermolecular distances. Due to this dense packing, especially as the density increases, an interpenetration of the short-range local HB network of the individual water molecules by non-hydrogen bonded neighbors starts to take place[21]. Another very interesting effect takes place at the Frenkel line. At lower densities than the one corresponding to the Frenkel line boundary (about 3.4 ρ_c) the dominating fractions f_n of hydrogen bonded water molecules (n is the number of hydrogen bonds formed by a water molecule) are f_2 and f_1. However, when crossing the Frenkel line the fraction f_3 becomes the dominating one. At the Frenkel line, three intersections between different $f_n(\rho)$ curves are also observed. More specifically, at the Frenkel line $f_2 \approx f_3$, $f_1 \approx f_4$, and $f_0 \approx f_5$, respectively[21]. All these findings are clear indications that the local structural environments in SCW change significantly when crossing the Frenkel line. Therefore, this blueshift of the isosbestic points of the rotational and translational DOS by about 150 and 100 cm^{-1}, respectively, can be considered as another indication of the change in the molecular-scale structural and dynamic phenomena when crossing the Frenkel line. This new finding can motivate experimentalists to investigate possible similar effects in a wide range of spectroscopic properties of supercritical water and other molecular systems, providing strong experimental evidence about the existence and the exact location of the Frenkel line. As previously mentioned, after crossing the Frenkel line (at about 3.4 ρ_c and 1.17 GPa) the system at 8.5 GPa converts through a first-order phase transition to a fcc plastic crystal phase[21]. In Figure 3 we present the changes in the entropic components S_{trans}

and S_{rot}, their sum $S_{trans} + S_{rot}$, as well as the ratio S_{rot} / S_{trans} at the pressure range 1.17-11 GPa.

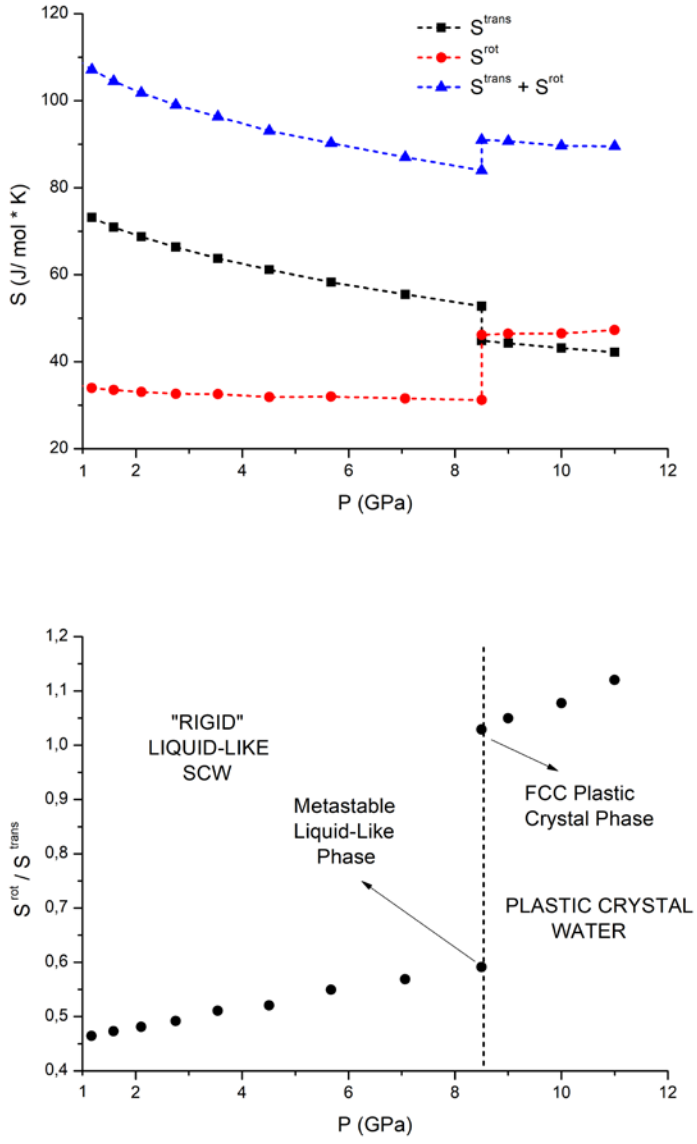

Figure 3: Pressure dependence of S^{rot}, S^{trans}, their sum and ratio when going from the rigid liquid-like phase to the fcc plastic crystal phase.

From Figure 3 it can be clearly seen that in the pressure range 1.17-8.5 GPa the decrease of the rotational component S^{rot} is very small, whereas the decrease of S^{trans} is much more pronounced. However, when crossing the melting line, a discontinuous significant increase of S^{rot} and a smaller discontinuous decrease of S^{trans} and discontinuous increase of the total

entropy are observed. In the pressure range 8.5-11 GPa, where the system is in the fcc plastic crystal phase, S^{rot} slightly increases and S^{trans} slightly decreases with the pressure increase, respectively. The total entropy of the plastic crystal phase slightly decreases with the pressure increase at the investigated pressure range. These changes are also very clearly reflected on the ratio S^{rot} / S^{trans}. In the pressure range 1.17 -8.5 GPa, where SCW is in the rigid liquid-like phase, this ratio increases from about 0.46 to 0.59. However, when the first-order phase transition from the metastable liquid-like phase to the fcc plastic crystal phase takes place at 8.5 GPa (with a corresponding Gibbs free energy change $\Delta G \simeq -7 \quad kJ / mol$ [21]), then the S^{rot} / S^{trans} jumps from the 0.59 to the 1.03 value. Therefore, in the fcc plastic crystal phase the translational component of the entropy is no longer the dominant one. When crossing the melting line, the S^{rot} / S^{trans} ratio increases almost linearly with the pressure up to the value of 1.12 at 11 GPa. This increase of the ratio S^{rot} / S^{trans} can be interpreted due to the very hindered translational dynamics of the water molecules in the fcc plastic crystal phase, especially when the pressure increases. All these findings clearly signify the role of entropy as a fingerprint of the observed structural and first-order phase transitions taking place along a near-critical isotherm of SCW.

The changes in the rotational and translational dynamics of water when crossing the melting line are also reflected on the corresponding DOS. The changes in the rotational and translational DOS $s_{rot}(v)$ and $s_{trans}(v)$ when crossing the melting line and going from the metastable liquid-like phase at 8.5 GPa to the fcc plastic crystal phase at the pressure range 8.5-11 GPa are presented in Figure 4. From this figure it can be clearly observed that the peak observed for $s_{rot}(v)$ at $v / c = 450 \quad cm^{-1}$ corresponding to the metastable liquid-like phase at 8.5 GPa, shifts towards lower frequencies, around $v / c = 400 \quad cm^{-1}$ in the fcc plastic crystal phase.

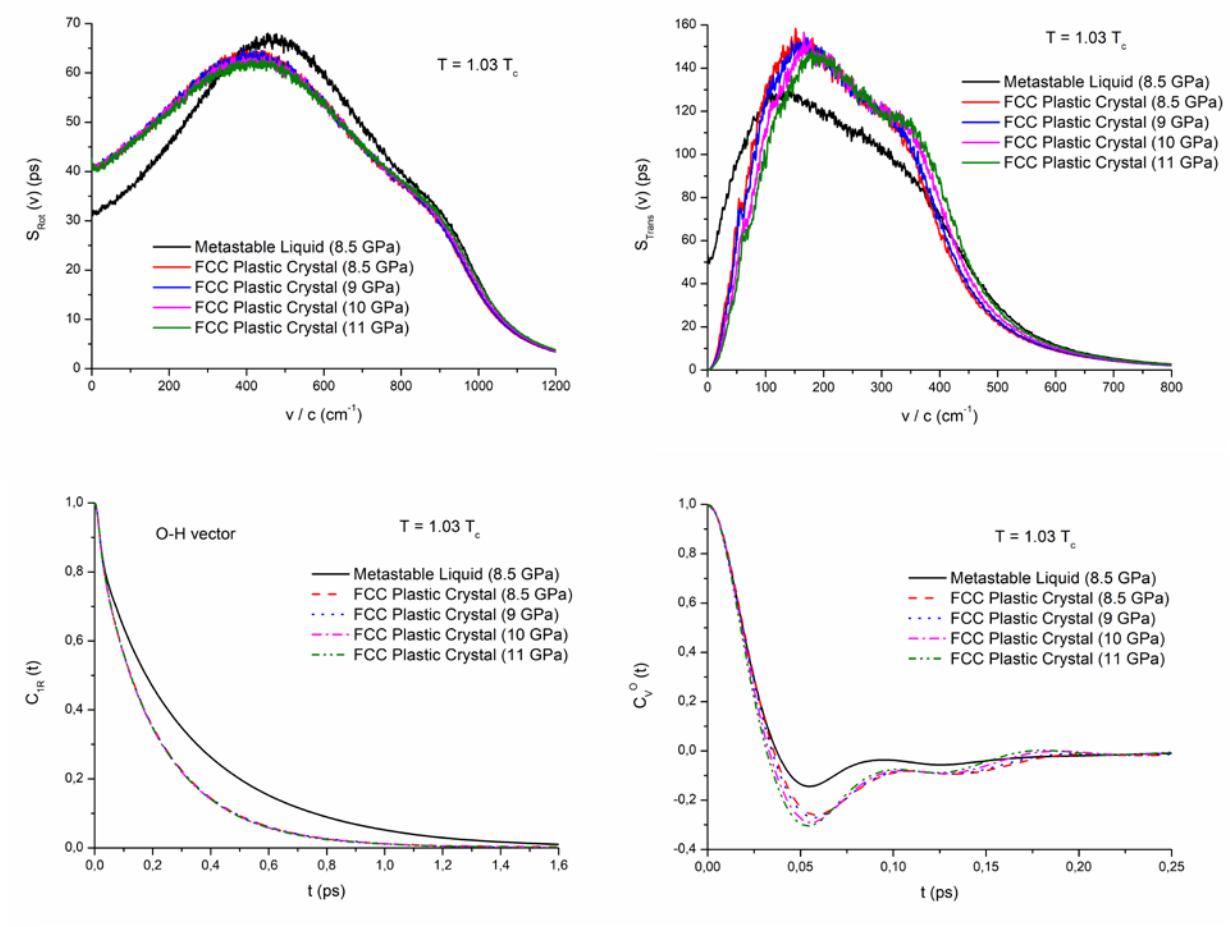

Figure 4: Calculated rotational and translational DOS for the metastable liquid-like and the fcc plastic crystal phase of SCW water (top panel) in the pressure range 8.5-11 GPa. The corresponding calculated first-order Legendre reorientational tcf $C_{1R}(t)$ for the O-H vectors of the water molecules and the oxygen atomic velocity tcf $C_v^{O}(t)$ (bottom panel) are also displayed.

This is a clear indication that molecular rotation in the plastic crystal phase becomes less hindered in comparison with the liquid-like phase. In the fcc plastic crystal phase, the pressure effects upon the position of this low-frequency peak are very weak. The high-frequency shoulder observed at about $v/c = 900 \;\; cm^{-1}$ remains almost unchanged when going from the liquid-like phase to the plastic crystal one. These findings indicate that the pressure effects upon molecular rotation in the plastic crystal phase are not very strong. This was further evidenced by calculating the average first-order Legendre reorientational

tcf $C_{1R}(t)$ and the corresponding correlation time τ_{1R} for the two O-H intramolecular vectors of the water molecules:

$$C_{1R}(t) = \left\langle \vec{u}_i(0) \cdot \vec{u}_i(t) \right\rangle \quad , \quad \tau_{1R} = \int_0^\infty C_{1R}(t) \cdot dt \tag{14}$$

In Eq. 14 $\vec{u}_i$ is a O-H unit intramolecular vector associated with a molecule *i*. From Figure 4 it can be clearly seen that at the metastable liquid-like phase $C_{1R}(t)$ decays slower than at the fcc plastic crystal phase. This is also reflected on the calculated correlation times τ_{1R} . The corresponding τ_{1R} values at 8.5 GPa for the liquid-like and the plastic crystal phase are 0.30 and 0.20 ps, respectively. This means that O-H reorientation in the plastic crystal phase is faster. However, in the plastic crystal phase, up to pressures of 11 GPa, the calculated reorientational tcfs are almost identical, signifying that in this particular pressure range molecular reorientation is not affected by the pressure increase. On the other hand, the translational dynamics is more hindered in the plastic crystal phase in comparison with the liquid-like one, and this is clearly reflected on both the translational DOS and the oxygen velocity tcfs. The low-frequency peak of $S_{trans}(v)$ shifts from $v/c = 125 \ \ cm^{-1}$ in the metastable liquid-like phase at 8.5 GPa to $v/c = 150 \ \ cm^{-1}$ in the fcc plastic crystal phase at the same pressure. As the pressure increases, a further blueshift of this peak is observed, with a peak corresponding to $v/c = 179 \ \ cm^{-1}$ at 11 GPa. Moreover, in the plastic crystal phase a shoulder appears at higher frequencies, around $v/c = 350 \ \ cm^{-1}$, which becomes more pronounced as the pressure increases. All these findings are clear manifestations of the more hindered translational dynamics in the fcc plastic crystal phase. This behavior is also reflected on the shape of the calculated oxygen velocity tcfs $C_v^{\,O}(t)$, with a more pronounced negative part in the case of the plastic crystal phase, particularly as the pressure increases.

Apart from all these fingerprints of the crossing of the Frenkel and melting line of water on the thermodynamic and dynamic properties of water at near-critical, supercritical conditions, we observed another very interesting behavior of the dielectric constant of

water when crossing the melting line at about 8.5 GPa. The static dielectric constant ε_0 of water was calculated using the following formalism[38,50]:

$$\varepsilon_0 = \varepsilon_\infty + 3yG_K \tag{15}$$

where ε_∞ is the dielectric constant at optical frequencies, approaching the value 1 at high frequencies because we assumed rigid non-polarizable molecules, and y is the dimensionless dipolar strength defined as:

$$y = \frac{4\pi\rho\vec{\mu}^2}{9k_BT} \tag{16}$$

with ρ is the number density of water and $\vec{\mu}$ the molecular dipole vector. In addition, G_K is the finite system Kirkwood factor given by

$$G_K = \frac{\left\langle \vec{M}^2 \right\rangle}{\left\langle N \cdot \vec{\mu}^2 \right\rangle} \tag{17}$$

where $\vec{M} = \sum_{i=1}^{N} \vec{\mu}_i$ is the total dipole moment of all the molecules N in the system. The pressure dependence of the static dielectric constant of water in the pressure range 0.12 - 11 GPa is presented in Figure 5. From this figure it can be seen that in the “non-rigid” (or “soft”) liquid phase the static dielectric constant increases with the pressure increase from the value of about 16 at 0.12 GPa to 30 at 1.17 GPa, where the Frenkel line is crossed. In the rigid-liquid phase, the dielectric constant increases less rapidly with the pressure increase. From the value of 30 at 1.17 GPa, the static dielectric constant increases up to 53 at the metastable liquid-like phase at 8.5 GPa. However, during the transition to the fcc plastic crystal phase a significant jump of the dielectric constant to a value of about 68 is observed, which further increases with the pressure up to the value of about 78 at 11 GPa. This discontinuous change in the dielectric constant when crossing the melting line and its significant increase in the plastic crystal phase in comparison with the rigid-liquid phase

could be attributed to the different orientational ordering of the molecular dipole vectors of the water molecules in the crystal phase. This is directly reflected on the discontinuous change in the value of the finite Kirkwood factor G_K when crossing the melting line. The values of G_K corresponding to the metastable liquid-like phase and the fcc plastic crystal phase at 8.5 GPa are 3.83 and 4.75, respectively. This change corresponds to a ≈ 24 % increase of G_K, which is consistent with the corresponding ≈ 28% increase of the static dielectric constant (from the value of 53 to 68). Note that the corresponding density change upon the transition from the metastable liquid-like phase to the plastic crystal phase (from 4.976 ρ_c to 5.178 ρ_c) is around 4 %, signifying that the changes in the dipole orientations play the most important role in the change of the dielectric constant. The changes in the rotational entropy of the system are most likely related to these changes in the orientational ordering of the water molecules in the plastic crystal phase, since they both exhibit a discontinuous significant increase when the melting line is crossed.

Note also that the observation of plastic crystal polymorphs of water at subcritical and supercritical temperatures and high pressures has been reported only in simulation studies so far[50-54]. Previous experimental studies have reported a first order phase transition from liquid water to a solid phase at 400 K and pressures above 7 GPa[55], as well as the existence of a new crystal phase in the pressure range from 20 to 42 GPa and a wide temperature range[56]. However, the structure of these phases could not be identified and their experimental identification is very challenging. From this point of view, this particular fingerprint of the crossing of the melting line towards a plastic crystal phase on the dielectric properties of water revealed in the present study, in terms of this discontinuous jump of the dielectric constant, could provide very useful guidelines for future experiments to identify these plastic crystal phases of water.

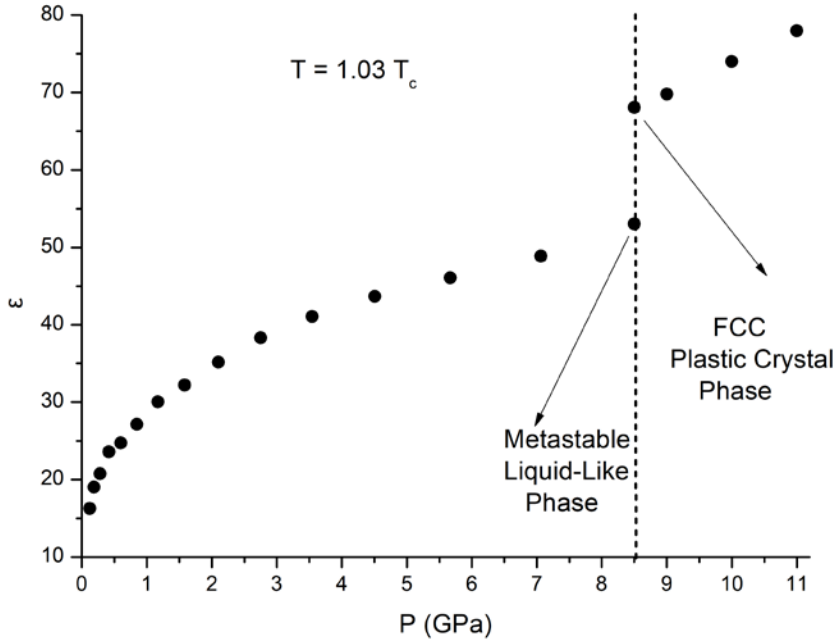

Figure 5: Pressure dependence of the static dielectric constant of water in the range 0.12 - 11 GPa.

Summing up in brief our concluding remarks, we may say that our findings reveal for the first time some very characteristic fingerprints of the crossing of the Frenkel and melting line on the properties of high-pressure water at a near critical temperature (1.03 T_c), providing deeper insight of the molecular scale mechanisms taking place when crossing these lines. At the same time, our findings can be used as important guidelines to theoreticians and experimentalists working on the identification of the structural and first-order transitions taking place in water at high temperature and pressure conditions, aiming to understand a wide range of phenomena with real and important applications in chemistry, physics and earth-planetary science.

Acknowledgements

The use of the computational facilities of the Computer Simulation in Condensed Matter Research Group (SIMCON) at the Physics Department of the Technical University of Catalonia (UPC) and of the Physical Chemistry Laboratory at the Chemistry Department of the National and Kapodistrian University of Athens (NKUA) is gratefully

acknowledged. E. G. acknowledges financial support from the Ministerio de Ciencia, Innovación y Universidades of Spain, Grant PGC2018-099277-B-C21 (MCIU/AEI/ERDF).

References

1) Besnard, M.; Tassaing, T.; Danten, Y.; Andanson, J. M.; Soetens, J. C.; Cansell, F.; Loppinet-Serani, A.; Reveron, H.; Aymonier, C. Bringing together fundamental and applied science: The supercritical fluids route. *J. Mol. Liq.* **2006**, *125*, 88-99.

2) Simeoni, G.G.; Bryk, T.; Gorelli, F.A.; Krisch, M.; Ruocco, G.; Santoro, M.; Scopigno, T. The Widom line as the crossover between liquid-like and gas-like behaviour in supercritical fluids. *Nat. Phys.* **2010**, *6*, 503-507.

3) McMillan, P. F.; Stanley, H.E. Going supercritical. *Nat. Phys.* **2010**, *6*, 479-480.

4) Brazhkin, V.V., Fomin, Y.D.; Lyapin, A.G.; Ryzhov, V.N.; Tsiok, E.N. Widom line for the liquid-gas transition in Lennard-Jones system. *J. Phys. Chem. B* **2011**, *115*, 14112-14115.

5) Gorelli, F.A.; Bryk, T.; Krisch, M.; Ruocco, G.; Santoro, M.; Scopigno, T. Dynamics and Thermodynamics beyond the critical point. *Sci. Rep.* **2013**, *3*, 1203.

6) Gallo, P.; Corradini, D.; Rovere, M. Widom line and dynamical crossovers as routes to understand supercritical water. *Nat. Commun.* **2014**, ***5***, 586.

7) Maxim, F.; Contescu, C.; Boillat, P.; Niceno, B.; Karalis, K.; Testino, A. Visualization of supercritical water pseudo-boiling at Widom line crossover. *Nat. Commun.* **2019**, *10*, 4114.

8) Karalis, K.; Ludwig, C.; Niceno, B. Supercritical water anomalies in the vicinity of the Widom line. *Sci. Rep.* **2019**, *9*, 15731.

9) Ha, M.Y.; Yoon, T. J.; Tlusty, T.; Jho, Y.; Lee, W. B. Widom Delta of Supercritical Gas–Liquid Coexistence. *J. Phys. Chem. Lett.* **2018**, *9*, 1734-1738.

10) Corradini, D.; Rovere, M.; Gallo, P. The Widom line and dynamical crossover in supercritical water: Popular water models versus experiments. *J. Chem. Phys.* **2015**, *143*, 114502.

11) Strong, S.E.; Shi, L.; Skinner, J.L.; Percolation in supercritical water: Do the Widom and percolation lines coincide? *J. Chem. Phys.* **2018**, *149*, 084504.

12) Cockrell, C.; Brahzkin, V.V; Trachenko, K. Transition in the supercritical state of matter: Review of experimental evidence. *Phys. Rep.* **2021**, *941*, 1-27.

13) Brazhkin, V.V.; Fomin, Yu. D.; Lyapin, A.G.; Ryzhov, V.N.; Trachenko, K. Two liquid states of matter: A dynamic line on a phase diagram. *Phys. Rev. E* **2012**, *85*, 031203.

14) Bolmatov, D.; Brazhkin, V.V.; Trachenko, K. Thermodynamic behaviour of supercritical matter. *Nat. Commun.* **2013**, *4*, 2331.

15) Brazhkin, V.V.; Fomin, Yu. D.; Lyapin, A.G.; Ryzhov, V.N.; Tsiok, E.N.; Trachenko, K. "Liquid-Gas" Transition in the Supercritical Region: Fundamental Changes in the Particle Dynamics. *Phys. Rev. Lett.* **2013**, *111*, 145901.

16) Yang, C.; Brazhkin, V.V.; Dove, M.T.; Trachenko, K. Frenkel line and solubility maximum in supercritical fluids. *Phys. Rev. E* **2015**, *91*, 012112.

17) Tucker, S.C. Solvent Density Inhomogeneities in Supercritical Fluids. *Chem. Rev.* **1999**, *99*, 391-418.

18) Cockrell, C.; Brazhkin, V.V.; Trachenko, K. Universal interrelation between dynamics and thermodynamics and a dynamically driven "c" transition in fluids. *Phys. Rev. E* **2021**, *104*, 034108.

19) Proctor, J.E.; Pruteanu, C.G.; Morrison, I.; Crowe, I.F.; Loveday, J.S. Transition from Gas-like to Liquid-like Behavior in Supercritical N_2. *J. Phys. Chem. Lett.* **2019**, 10, 6584-6589.

20) Banuti, D.T. Crossing the Widom-line–supercritical pseudo-boiling. *J. Supercrit. Fluids* **2015**, *98*, 12-16.

21) Skarmoutsos, I.; Henao, A.; Guardia, E.; Samios, J. On the Different Faces of the Supercritical Phase of Water at a Near-Critical Temperature: Pressure-Induced Structural Transitions Ranging from a Gaslike Fluid to a Plastic Crystal Polymorph. *J. Phys. Chem. B* **2021**, *125*, 10260-10272.

22) Skarmoutsos, I.; Dellis, D.; Samios, J. The Effect of Intermolecular Interactions on Local Density Inhomogeneities and Related Dynamics in Pure Supercritical Fluids. A Comparative Molecular Dynamics Simulation Study. *J. Phys. Chem. B* **2009**, *113*, 2783-2793.

23) Bryk, T.; Gorelli, F.A.; Mryglod, I.; Ruocco, G.; Santoro, M.; Scopigno, T. Behavior of Supercritical Fluids across the "Frenkel Line". *J. Phys. Chem. Lett.* **2017**, *8*, 4995-5001.

24) Brazhkin, V.V.; Prescher, C.; Fomin, Yu. D.; Tsiok, E. N.; Lyapin, A. G.; Ryzhov, V. N.; Prakapenka, V.B.; Stefanski, J.; Trachenko, K.; Sapelkin, A. Comment on "Behavior of Supercritical Fluids across the 'Frenkel Line'. *J. Phys. Chem. B* **2018**, *122*, 6124–6128.

25) Bryk, T.; Gorelli, F.A.; Mryglod, I.; Ruocco, G.; Santoro, M.; Scopigno, T. Reply to "Comment on 'Behavior of Supercritical Fluids across the Frenkel Line'. *J. Phys. Chem. B* **2018**, *122*, 6120-6123.

26) Cockrell, C.J.; Dicks, O.; Wang, L.; Trachenko, K.; Soper, A.K.; Brazhkin, V.V.; Marinakis, S. Experimental and modeling evidence for structural crossover in supercritical CO_2. *Phys. Rev. E* **2020**, 101, 052109.

27) Pruteanu, C.G.; Proctor, J.E.; Alderman, O.L.G.; Loveday, J.S. Structural Markers of the Frenkel Line in the Proximity of Widom Lines. *J. Phys. Chem. B* **2021**, *125*, 8902-8906.

28) Pruteanu, C.G.; Kirsz, M.; Ackland, G.J. Frenkel Line in Nitrogen Terminates at the Triple Point. *J. Phys. Chem. Lett.* **2021**, *12*, 11609-11615.

29) Yoon, T.J.; Ha, M.Y.; Lee, W.B.; Lee. Y.-W. "Two-Phase" Thermodynamics of the Frenkel Line. *J. Phys. Chem. Lett.* **2018**, 9, 4550-4554.

30) Yoon, T.J.; Ha, M.Y.; Lazar, E.A.; Lee, W.B.; Lee. Y.-W. Topological Characterization of Rigid–Nonrigid Transition across the Frenkel Line. *J. Phys. Chem. Lett.* **2018**, *9*, 6524-6528.

31) Yoon, J.T.; Patel, L.A; Ju, T.; Vigil, M.J.; Findikoglu, A.T.; Currier, R.P.; Maerzke, K.A. Thermodynamics, dynamics, and structure of supercritical water at extreme conditions. *Phys. Chem. Chem. Phys.* **2020**, *22*, 16051-16062.

32) Lin, S.-T.; Blanco, M.; Goddard, W.A., III The Two-Phase Model for Calculating Thermodynamic Properties of Liquids from Molecular Dynamics: Validation for the Phase Diagram of Lennard-Jones Fluids. *J. Chem. Phys.* **2003**, *119*, 11792-11805.

33) Lin, S.-T.; Maiti, P.K.; Goddard, W.A., III Two-Phase Thermodynamic Model for Efficient and Accurate Absolute Entropy of Water from Molecular Dynamics Simulations. *J. Phys. Chem. B* **2010**, *114*, 8191-8198.

34) Berendsen, H.J.C.; Grigera, J.R.; Straatsma, T.P. The missing term in effective pair potentials. *J. Phys. Chem.* **1987**, *91*, 6269-6271.

35) Skarmoutsos, I.; Guardia, E.; Samios, J. Local structural fluctuations, hydrogen bonding and structural transitions in supercritical water. *J. Supercrit. Fluids* **2017**, *130*, 156-164.

36) Guissani, Y.; Guillot, B. A computer simulation study of the liquid-vapor coexistence curve of water. *J. Chem. Phys.* **1993**, *98*, 8221-8235.

37) Alejandre, J.; Tildesley, D.J. Molecular dynamics simulation of the orthobaric densities and surface tension of water. *J. Chem. Phys.* **1994**, *102*, 4574-4583.

38) Guardia, E.; Marti, J. Density and temperature effects on the orientational and dielectric properties of supercritical water. *Phys. Rev. E* **2004**, *69*, 011502.

39) Smith, W.; Forester, T.R. DL_POLY_2.0: A general-purpose parallel molecular dynamics simulation package. *J. Mol. Graph.* **1996**, *14*, 136-141.

40) Allen, M. P.; Tildesley, D. J. *Computer Simulations of Liquids*, Oxford University Press, Oxford, 1987.

41) Hoover, W.G. Canonical dynamics: Equilibrium phase-space distributions. *Phys. Rev. A* **1985**, *31*, 1695-1697.

42) Hoover, W.G. Constant-pressure equations of motion. *Phys. Rev. A* **1986**, *34*, 2499-2500.

43) Caro, M.A.; Laurila, T.; Lopez-Acevedo, O. Accurate schemes for calculation of thermodynamic properties of liquid mixtures from molecular dynamics simulations. *J. Chem. Phys.* **2016**, *145*, 244504.

44) Kumar, H.; Mukherjee, B.; Lin, S.-T.; Dasgupta, C.; Sood, A.K.; Maiti, P.K. Thermodynamics of water entry in hydrophobic channels of carbon nanotubes. J. *Chem. Phys.* **2011**, *134*, 124105.

45) Fomin, Y.D.; Ryzhov, V.N.; Tsiok, E.N.; Brazkhin, V.V.; Trachenko, K. Crossover of collective modes and positive sound dispersion in supercritical state. *J. Phys.: Condens. Matter* **2016**, *28*, 43LT01.

46) Greger, M.; Kollar, M. and D. Vollhardt, Isosbestic points: How a narrow crossing region of curves determines their leading parameter dependence. *Phys. Rev. B* **2013**, *87*, 195140.

47) Berlett, B.S.; Levine, R.L.; Stadtman, E.R. Use of Isosbestic Point Wavelength Shifts to Estimate the Fraction of a Precursor That Is Converted to a Given Product. *Anal. Biochem.* **2000**, 287, 329-333.

48) Errington, J.R.; Debenedetti, P. G. Relationship between structural order and the anomalies of liquid water. *Nature* **2001**, *409*, 318–321.

49) Henchman, R.H.; Cockram, S. J. Water's non-tetrahedral side. *Faraday Discuss.* **2013**, 167, 529-550.

50) Skarmoutsos, I.; Mossa, S.; Guardia, E. The effect of polymorphism on the structural, dynamic and dielectric properties of plastic crystal water: A molecular dynamics simulation perspective. *J. Chem. Phys.* **2019**, *150*, 124506.

51) Takii, Y.; Koga, K.; Tanaka, H. A plastic phase of water from computer simulation. *J. Chem. Phys.* **2008**, *128*, 204501.

52) Aragones, J. L.; Vega, C. Plastic crystal phases of simple water models. *J. Chem. Phys.* **2009**, *130*, 244504.

53) Adachi, Y.; Koga, K. Structure and phase behavior of high-density ice from molecular-dynamics simulations with the ReaxFF potential. *J. Chem. Phys.* **2020**, *153*, 114501.

54) Hernandez, J.-A.; Caracas, R. Proton dynamics and the phase diagram of dense water ice. *J. Chem. Phys.* **2018**, *148*, 214501.

55) Dolan, D.; Knudson, M.; Hall, C.; Deeney, C. A metastable limit for compressed liquid water. *Nat. Phys.* **2007**, *3*, 339-342.

56) Schwager, B.; Boehler, R. H_2O: another ice phase and its melting curve. *High Press. Res.* **2008**, *28*, 431-433.